PREDICTION OF MOTION AND STRENGTH OF FLOATING MARINE STRUCTURES IN WAVES

SUHARA, Toshiro
Research Institute for Applied Mechanics, Kyushu University

TASAI, Fukuzo
Research Institute for Applied Mechanics, Kyushu University

MITSUYASU, Hisashi
Research Institute for Applied Mechanics, Kyushu University

MUTOH, Ikuo
Mitsui Ocean Development & Engineering Co., Ltd.

他

https://doi.org/10.5109/7173154

出版情報：Reports of Research Institute for Applied Mechanics. 22 (69), pp.15-45, 1974. 九州大学応用力学研究所

Reports of Research Institute for Applied Mechanics
Vol. XXII, 69, 1974

PREDICTION OF MOTION AND STRENGTH OF FLOATING MARINE STRUCTURES IN WAVES

By Toshiro SUHARA*, Fukuzo TASAI*
Hisashi MITSUYASU*, Ikuo MUTOH**
Eizo TANAKA**, Katsuto NAKASHIMA***
Kunihisa SAO** and Kyoichi INAOKA**

1. Introduction

Recently, in relation with ocean exploitation, various kinds of floating marine structures have been constructed one after the other.

Although these structures are complicated in shapes and are required to work under severe conditions, fundamental researches and technical experiences for such structures are not so exhaustive and comprehensive as those for ships. Therefore, in order to evaluate the motion and structural strength of such structures with sufficient accuracy, the conventional theoretical analysis and model tank test are considered to be not so sufficient, and it is necessary to investigate directly the response characteristics of structures against wave by measuring their motion and strength in the ocean simultaneously with the measurements of waves.

Taking an opportunity of construction of newly developed iron ore loading station with submersible, column stabilized, catamaran hulls, a systematic study was made on the motion and strength of the structure in waves. Theoretical analysis of the motion and strength of the structure was carried out first. Secondly, the theoretical results of its motion and longitudinal bending moment in waves were compared with that of model tank test. Thirdly, in order to check the theoretical calculation, the stress measurements were made at the time of launching. Finally, during the ocean towage of the structure from Japan to India, comprehensive measurements of motion of and stress in the structure in waves were conducted simultaneously with the accurate measurements of waves by means of a clover-leaf-buoy.

This report presents the method of predicting motion and strength of floating marine structures with sufficient accuracies through the above steps, when oceanic environmental conditions and working conditions are given.

* Research Institute for Applied Mechanics, Kyushu University.
** Mitsui Ocean Development & Engineering Co., Ltd.
*** Mitsui Shipbuilding & Engineering Co., Ltd.

It is noted that this report is mainly the detail of reference[1].

2. Outline of the Loading Station

The loading station "PRIYADARSHINI" which will be discussed in dealt this study (hereinafter referred to as L. S.) was constructed by Mitsui Ocean Development & Engineering Co., Ltd. for V. S. Dempo & Co. (Pvt.) Ltd., in Goa, India. The Port of Goa is shallow and large ore carriers cannot enter the port, and therefore, the loading for large ore carriers are performed at the offshore.

L. S. was designed to improve the loading and unloading operations at the offshore. It is grounded on the sea bed off the Port of Goa approximately 15 meter water depth. Iron ore is unloaded from small barges, accumulated on L. S., and loaded into a 60,000 DWT class ore carrier continuously. During the monsoon season, the operations are ceased, and L. S. is floated and towed into the Port for evacuation.

The Principal dimensions and general arrangement of L. S. are summarized as follows:

2.1. Principal dimensions

Type:	Submersible column stabilized catamaran type	
Lower hull:	Length (O. A.)	107.5m
	Width (O. A.)	32.0m
	Width (One hull)	10.0m
	Depth	5.0m
Column:	Length (Large)	7.5m
	(Small)	5.0m
	Width	10.0m
Upper deck:	Length (O. A.)	107.5m
	Width	32.0m
	Height	21.0m
Capacity:	Stock weigth	Approx. 19,000 ton
	Stock capacity	Approx. 9,400 cu. m.
Class:	† ABS Al Barge	

2.2 General arrangement[2]

L. S. consists of two rows of lower hulls, 14 columns built up on them and upper deck supported by the columns. (See Photo. 1.)

The lower hulls and columns of both sides are connected by triangle trusses.

Most of the lower hulls and columns are used for ballast tanks with approximately 20,000 tons.

Corresponding to the weight of iron ore stocked on the upper deck, the contact pressure to the sea bed can be adjusted by the ballast water.

The engine room and accommodation space are located on the upper

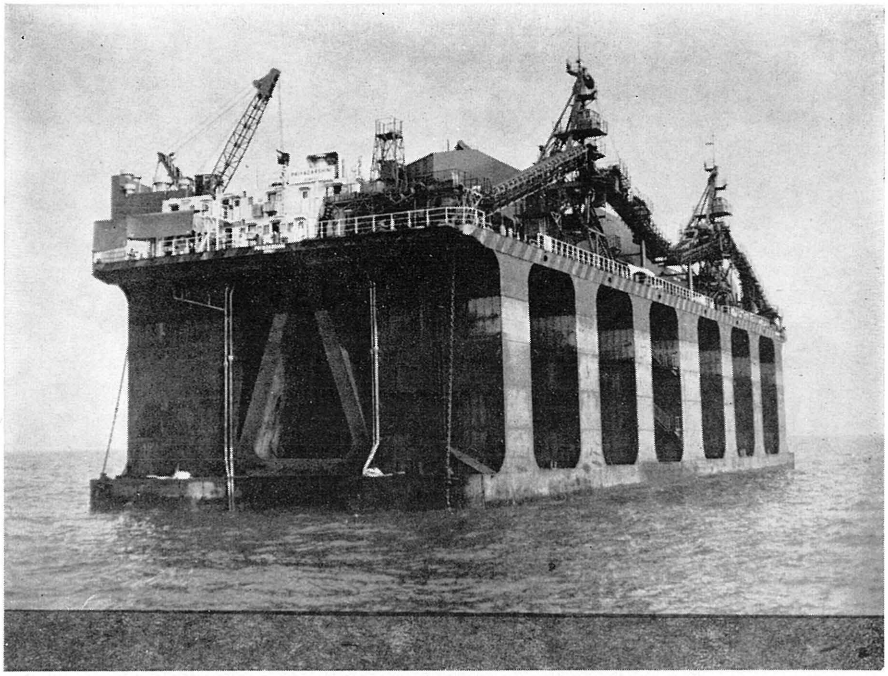

Photo. 1

(*Facing* p. 16)

deck, and the center portion of the upper deck is the stock yard where approximately 19,000 tons of iron ore can be stocked. In the port, three bucket cranes are installed for unloading iron ore from barges, and two sets

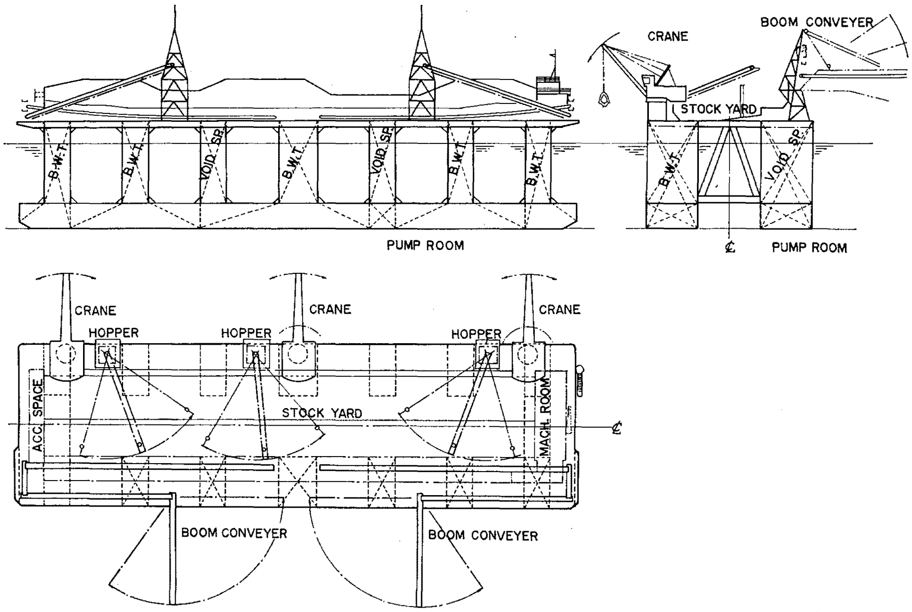

Fig. 1 General Arrangement

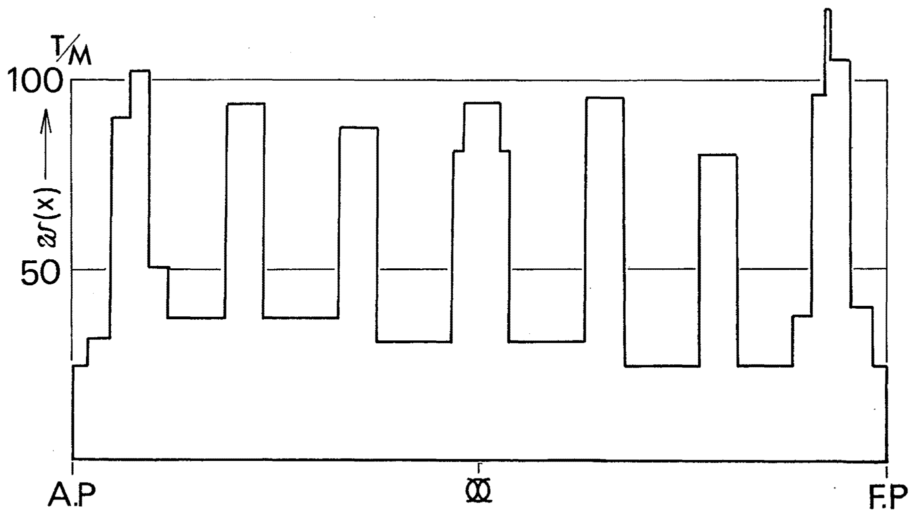

Fig. 2 Weight Distribution of L. S. at being towed

of belt conveyors and boom conveyors are installed in the starboard for loading the accumulated ore to an ore carrier.

Fig. 1, Fig. 2 and Fig. 3 show the general arrangement, weight distribution curve at the time of being towed and the midship section respectively.

Table 1 shows the principal particulars of L. S. used for the calculation described in the paper.

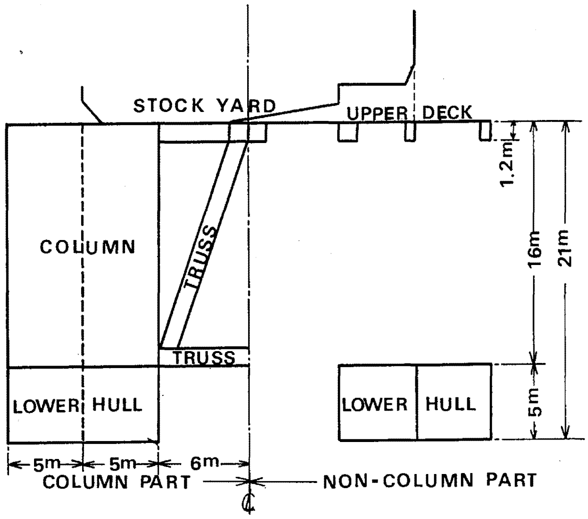

Fig. 3 Midship Section

3. Calculation Methods of Motion and Longitudinal Bending Moment

This Chapter presents the method of theoretical calculation of motion and longitudinal bending moment of catamaran hulls in oblique regular waves, and comparison of the calculation and experiment.

3.1 Theoretical calculation

The method of calculation used in this paper is the same as that used for calculating the motion of ordinary ships. That is, responses of periodic motions and longitudinal bending moment of the L. S. which advances with a constant speed in oblique regular waves are calculated by the strip method.[3] Results are illustrated in Fig. 4~Fig. 9.

Two dimensional radiation forces acting on the unit length of catamaran hull were calculated by Ohkusu's Method[4] which considered mutual hydrodynamic interaction between two cylinders. The diffraction pressure was calculated approximately in the same manner as in an ordinary ship. That is, for heave and pitch motions, diffraction pressure was approximately calculated by using orbital velocity and acceleration of incident wave at the depth of σT on the center line of the catamaran hull and for sway, yaw and roll motions, at the depth of T/2 on the center line. For catamaran such point of orbital motions are not existent in the hull. Then, in the case of 2p/T or 2b/T being large, this assumption is not suitable, and accuracy of calculation becomes worse in the high frequency area. Fig. 10 illustrates

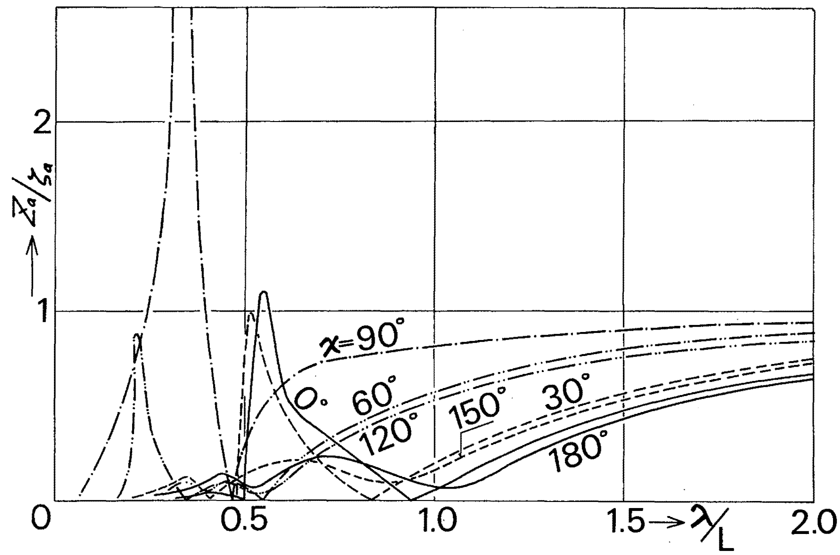

Fig. 4 Heave Amplitude (V=5KT)

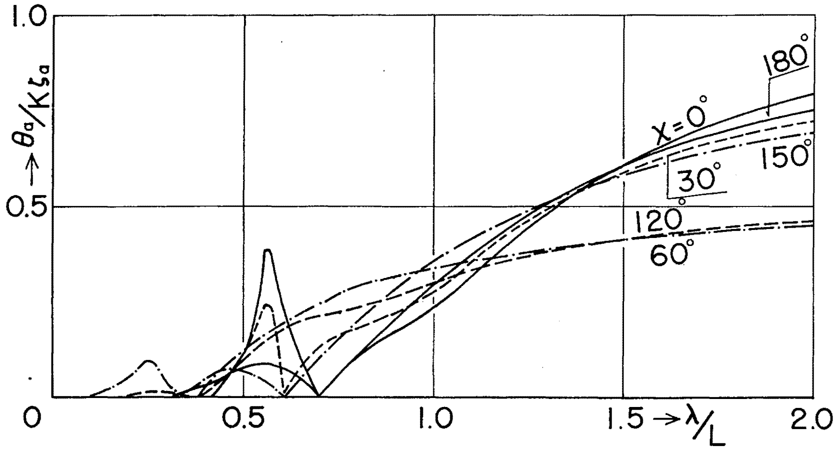

Fig. 5 Pitch Amplitude (V=5KT)

the comparison of the calculated value by the above approximate method for swaying amplitude in beam waves with "exact solution". Here, "exact solution" denotes a value obtained by using the wave exciting force that is calculated by the Haskind[5]-Bessho[6] 's equation, established between radiation force and wave exciting force.

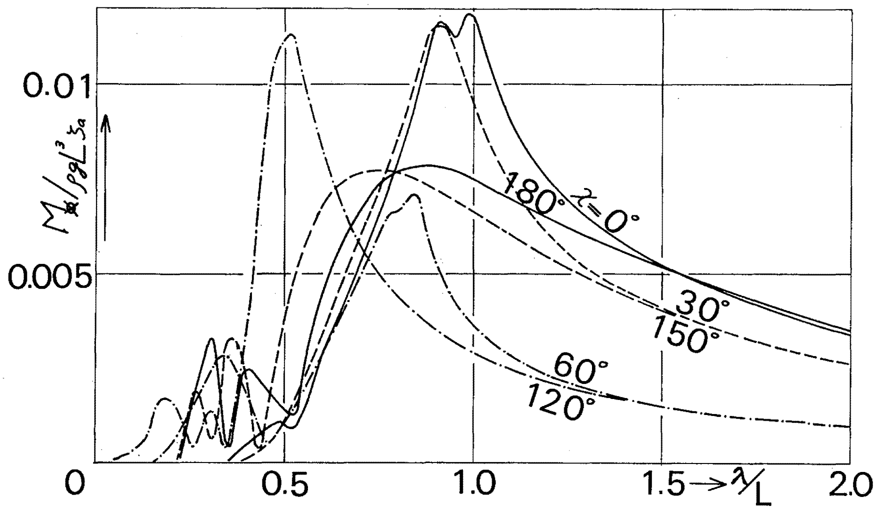

Fig. 6 Longitudinal bending Moment (V=5KT)

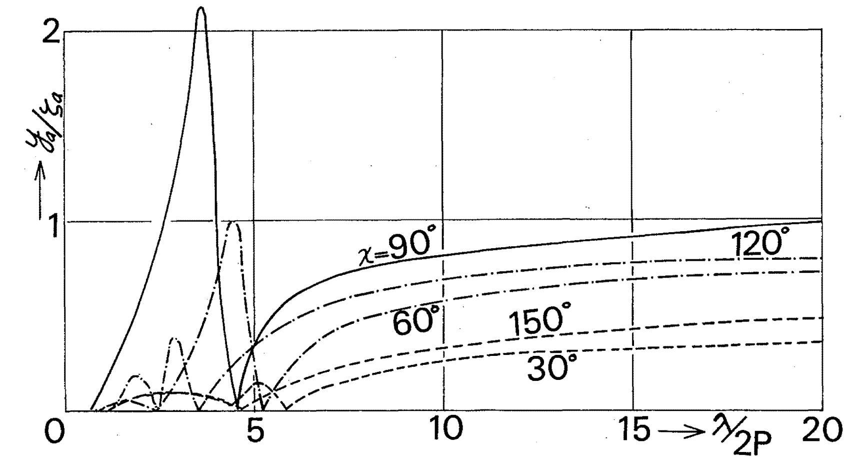

Fig. 7 Sway Amplitude (V=5KT)

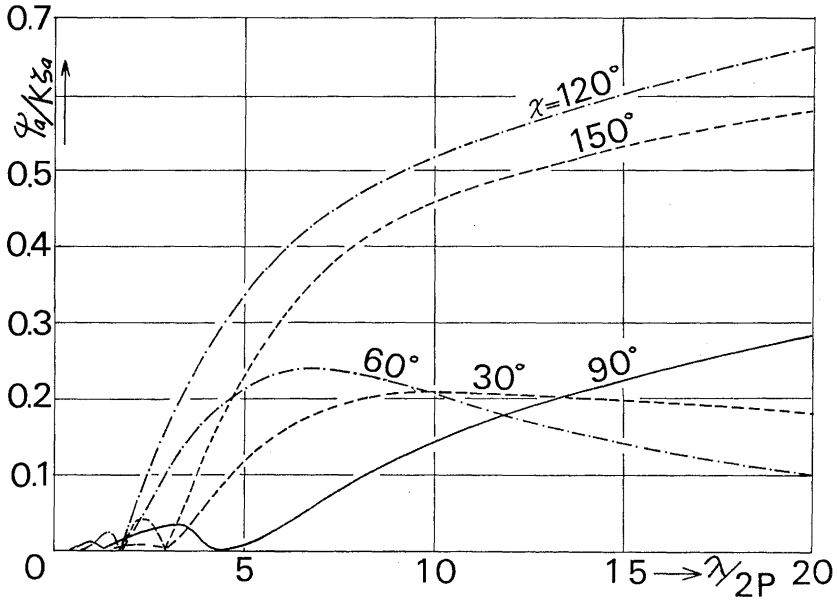

Fig. 8 Yaw Amplitude (V=5KT)

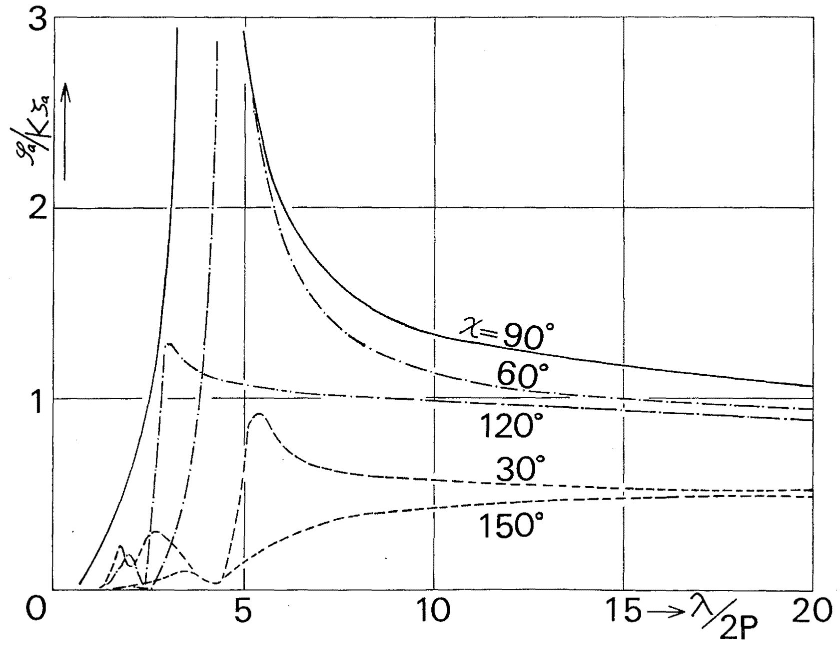

Fig. 9 Roll Amplitude (V=5KT)

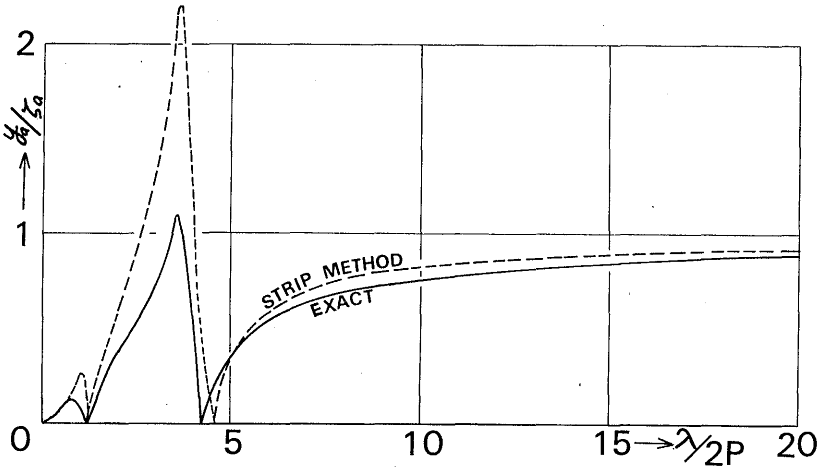

Fig. 10 Comparison between strip method solution and exact solution for sway amplitude

3.2 Tank test and correction of theoretical response function

This section presents the water tank tests conducted to examine accuracy of the theoretical calculation.

The tests were carried out in the towing tank ($L \times B \times D \times d = 80m \times 8m \times$

Table 1 Principal Particulars

DESCRIPTION		AT BEING TOWED	MODEL
Length between Perpendiculars	L	107.5m	2.15m
Breadth (Over All)	B	32.0m	0.64m
Depth (Keel to Upper Deck)	D	21.0m	0.42m
Draft	d	3.312m	0.05m
Displacement	W	7223t	48.48kg
Height of Center of Gravity above Keel	KG	12.26m	0.166m
Transverse Metacentric Height	GM	32.74m	0.748m
Distance of Center of Gravity from Midship	⊠G	−1.371m	0.0m
Radius of Longitudinal Gyration	Kyy	30.93m	0.607m
Radius of Transeverse Gyration	Kxx	14.0m	0.256m
Length Between Demihull Center Lines	2P	22.0m	0.44m
Breadth of Each Demihull	2b	10.0m	0.2m

3.5m×3m) of Sea Safety Research Laboratory of Research Institute for Applied Mechanics, Kyushu University, using a 1/50 scale model.

Principal particulars of the model are shown in Table 1. In head waves, heaving, pitching motions and longitudinal bending moments were measured at Froude number Fn=0.05 and 0.1, and in beam waves, heaving, rolling and swaying motions were measured under condition of Fn=0.

Ratio between wave heinght H_w and wave length λ was selected as follows;

$$1/40<H_w/\lambda<1/25 \quad \text{at} \quad 0.5<\lambda/L<0.7$$
$$1/70<H_w/\lambda<1/40 \quad \text{at} \quad \lambda/L>0.7$$

Comparison between theory and experiment are illustrated in Fig. 11~Fig. 13. Theoretical results in Fig. 13 are the values of exact solution.

As there were some differences between calculation and experiment especially in the relatively high frequency range, for the amplitude of the motion of L. S. which was towed in oblique waves at the speed of 5 knots (Fn=0.08) or less, the following correction coefficients were introduced for correcting the values calculated by the strip method in this paper.

(1) Pitching and heaving amplitude

Referring to Fig. 11 and Fig. 12, Kz and K_θ the correction coefficients for amplitudes of heaving and pitching motions of L. S. advancing on head waves with 5 KT (Fn=0.08) are determined as 0.33 for the high frequency range in which these amplitudes are extremum in head waves, and for other frequencies, no correction is made (Fig. 15).

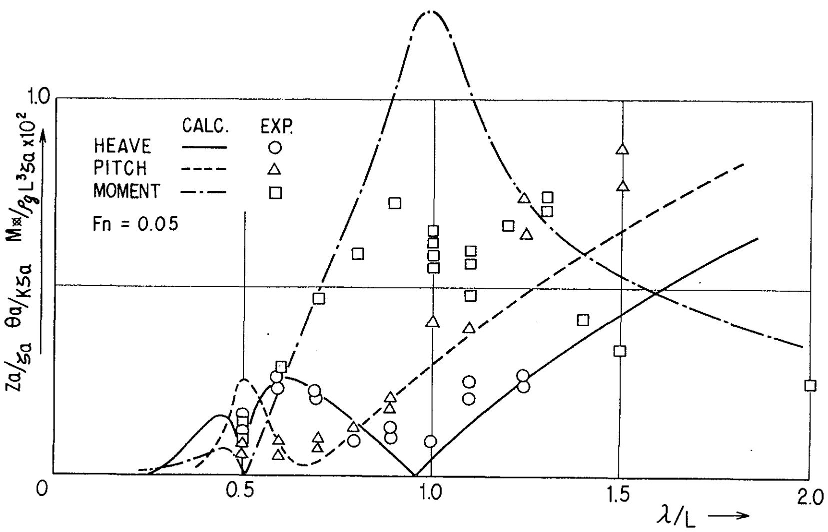

Fig. 11 Heave, Pitch and Longitudinal Bending Moment in Head Waves

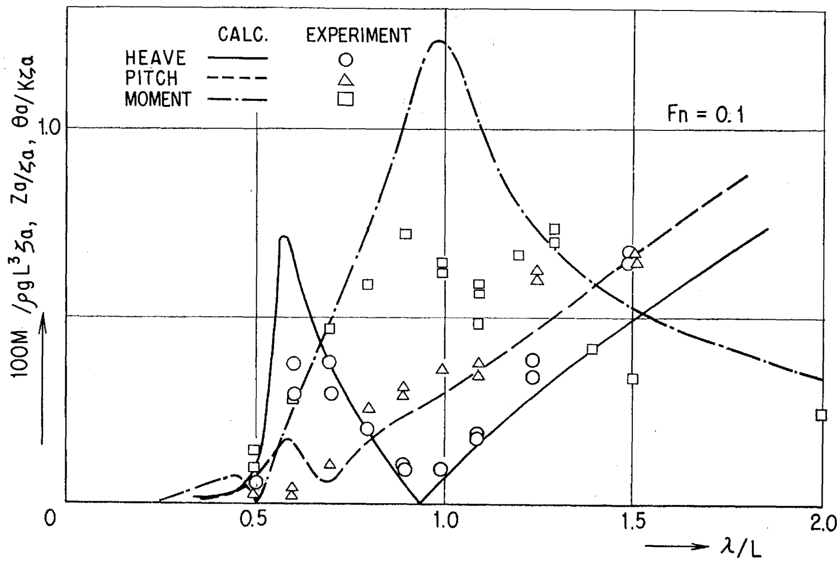

Fig. 12 Heave, Pitch and Longitudinal Bending Moment in Head Waves

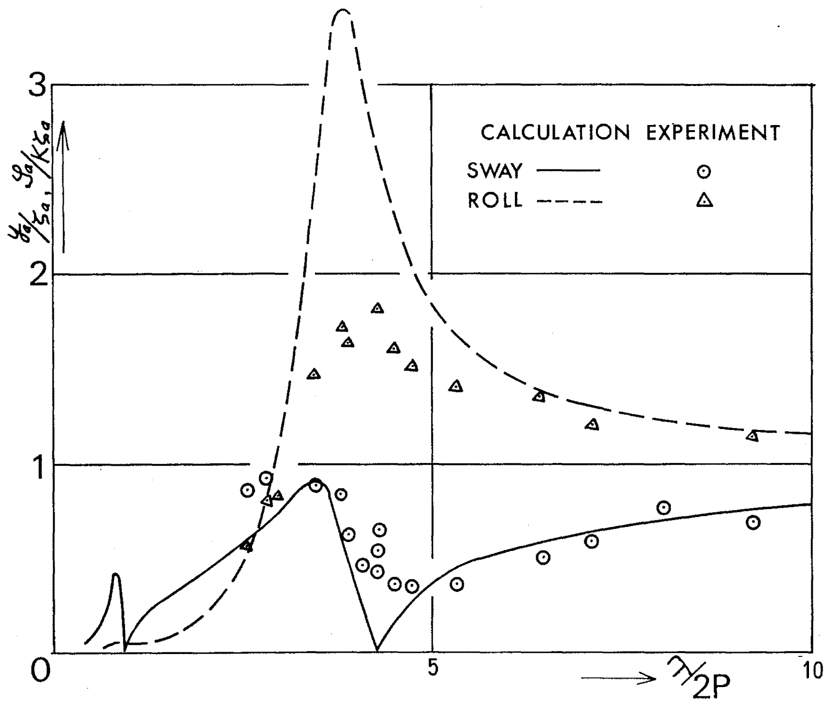

Fig. 13 Sway and Roll in Beam Waves

Assuming that the frequency characteristics of Kz and K_θ in oblique waves are the same as those in head waves, Kz and K_θ in Fig. 15 are applied for the correction coefficients of the longitudinal motions in oblique waves.

(2) Swaying amplitude of center of gravity

As shown in Fig. 13, the experimental results of swaying amplitudes in beam waves showed fairly good coincidence with that of exact solution.

On the other hand, as shown in Fig. 10, there are considerable difference in value between the exact solution and that calculated by the strip method for the range of small values of $\lambda/2p$.

Taking these results into consideration, for the extremum of swaying amplitude at high frequency range in oblique waves, the calculated value is multiplied by 0.5.

(3) Rolling amplitude

The experimental value at resonant frequency is approximately 60% of the theoretical exact value as shown in Fig. 13. Furthermore, similary to the case of swaying motion shown in Fig. 10, the amplitudes calculated by the strip method were larger than the exact ones and value of the latter is about 50% of the former at resonant frequency.

From these comparisons it results that $K\phi$ the correction coefficient becomes 0.3 at resonant frequncy in beam waves.

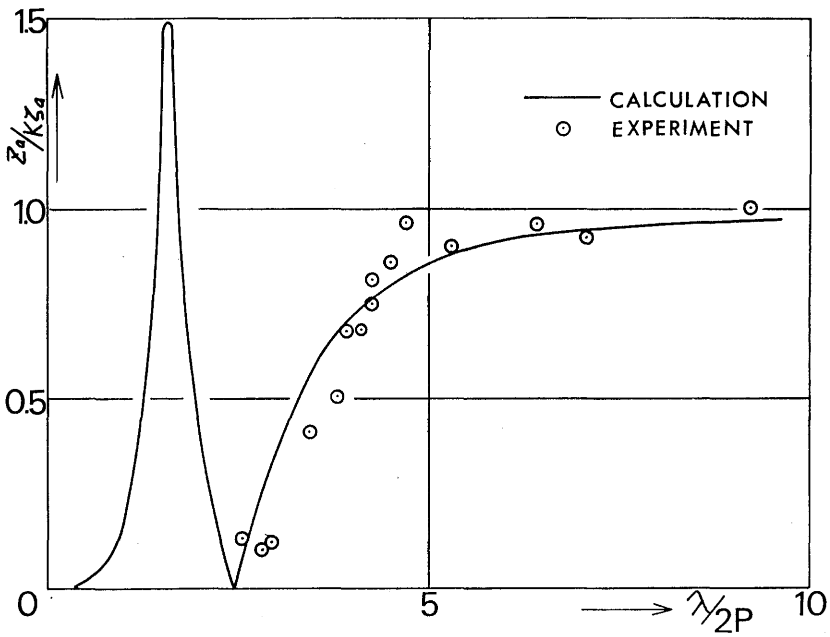

Fig. 14 Heave in Beam Waves

Referring to this result and that of Fig. 13, $K\phi$ illustrated in Fig. 15 is applied for rolling amplitude in oblique waves according to the same assumption as the longitudinal motions mentioned before.

(4) Amplitude of longitudinal bending moment

Based on the results shown in Fig. 11 and Fig. 12 and the same assumption as in the case of longitudinal motions, K_M the correction coefficient of the amplitide of longitudinal bending moment was determined and illustrated in Fig. 15.

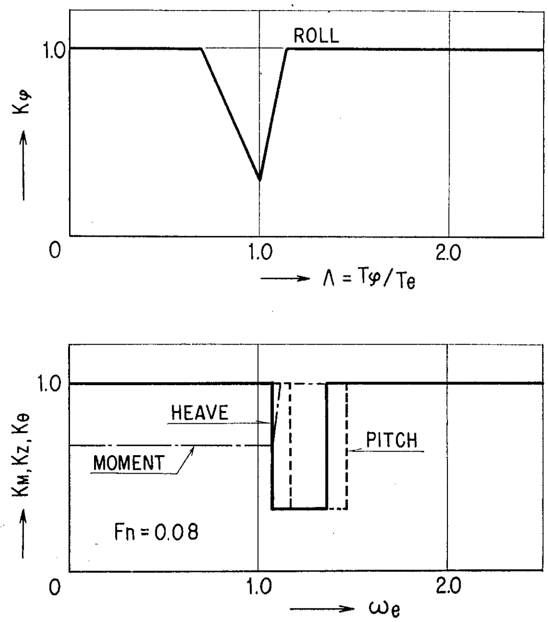

Fig. 15 Correction Coefficients

4. Method of Strength Calculation

On the longitudinal strength calculation, the finite element method using the large size elements was applied for both cases of this structure being assumed to be Rahmen structure and shell structure. These results of stress were compared with those measured at the time of launching, and the accuracies of calculation were examined respectively. As the result, for the longitudinal strength calculation of L. S. being towed in waves, shell structural finite element method was applied.

4.1 method of Longitudinal strength calculation

(1) Analysis of Rahmen structure

This structure is considered to be a two dimensional Rahmen structure as illustrated in Fig. 16, that is, the upper deck and two rows of lower hulls are each considered to be one beam, moreover, the columns in both sides and three connected trusses are considered to be one column, and thus, it can be assumed that the two beams mentioned above are connected by these seven columns. Longitudinal stress can be obtained by analyzing this Rahmen structure.

(2) Analysis of shell structure

Considering this structure to be a shell structure the shell structural finite element method was used. Its segments are illustrated in Fig. 16, and the dimensions of the elements were as follows:

Maximum size: 7.5×16m; Minimum size: 5×5m, Number of elements: 312 and Number of joints: 240 (considering structural symmetry).

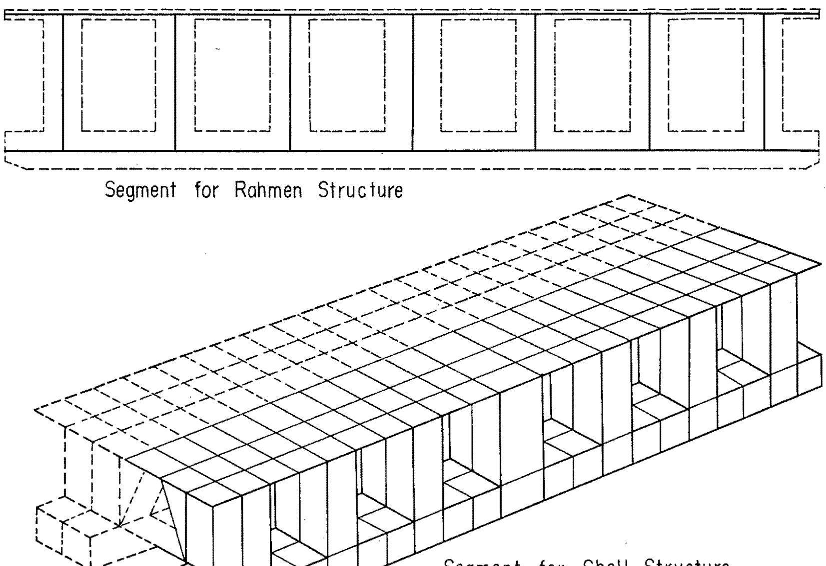

Fig. 16 Segment Illustration for Rahmen and Shell Structure

4.2 Comparison of calculated stress against measured stress at the time of launching

During the launching, longitudinal stresses were measured at 21 points total in the longitudinal and transverse cross-sections. In addition, vertical accelerations (on the center of upper deck at the midship and at the stern), launching speed and draft were also measured. Fig. 17 shows the shearing force and bending moment distribution curves calculated from the draft obtained by the photograph taken at the time of lift by the stern. Fig. 18 illustrates the comparison of the theoretically calculated values against those measured. As shown in Fig. 18, the values calculated as a shell structure are well coincide with the measured values except for the end portions of the structure, and the values calculated as a Rahmen structure is slightly smaller in general than those calculated as a shell structure, and at the lower hull top, some differences between these values are found. Based on these facts, overall strength can be calculated with fairly good accuracy even if large size elements are used as a shell structure. Moreover, it is available to calculate longitudinal strength approximately as a Rahmen structure at an initial design stage.

For the reason mentioned above, the finite element method for shell structure was applied to analyze longitudinal bending stress of L. S. in waves.

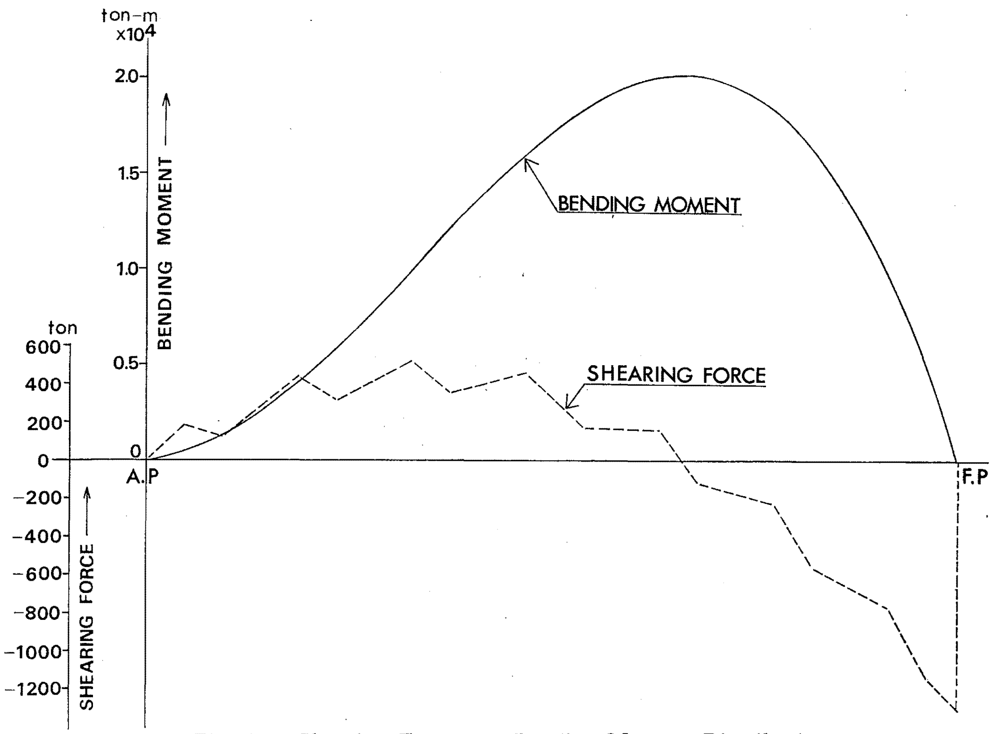

Fig. 17 Shearing Force and Bending Moment Distribution at Lift by the Stern

4.3 Longitudinal strength estimation method at sea experiment

When estimating stress of L. S. in waves, it is necessary to calculate frequency response function of stress by using the longitudinal wave bending moment obtained in the Chapter 3. However, the waves in a frequency range in which almost all powers of spectrum exist satisfy $\lambda/L>0.5$, and for such waves, longitudinal wave bending moment distribution is expressed approximately as $M=A\cos(\pi/Lx)+Bx^2+C$. The thick line in Fig. 19 indicates longitudinal wave bending moment at $\chi=150°$ and $\lambda/L=0.9$, and the dotted line indicates the approximate value of the above equation. Values of A, B and C differ depending upon χ and ω_e, but their ratio A:B:C is nearly constant.

Hence, if the stress distribution of the structure against this bending moment distribution is calculated by using the finite element method, frequency response functions of stress of all cross-sections can be determined.

Using the above equation, and supposing bending moment at midship is 10,000 ton-m, then, bending moment of the cross-section where strains were measured at the time of experiment in the ocean was 9,450 ton-m, and stress was 0.228 kg/sq. mm, and stress/bending moment wasl/41.5 (m^{-3}). For the analysis of the experiment in the ocean the function obtained by multiplying this proportional constant to the response function of bending moment was applied as the stress response function at that measuring point. However, structural shape at the time of the experiment in the ocean differed from that at the time of launching. As illustrated in Fig. 3, there existed the stock yard on the upper deck, and it affected longitudinal strength. However, in order to simplify the calculation, the stock yard was

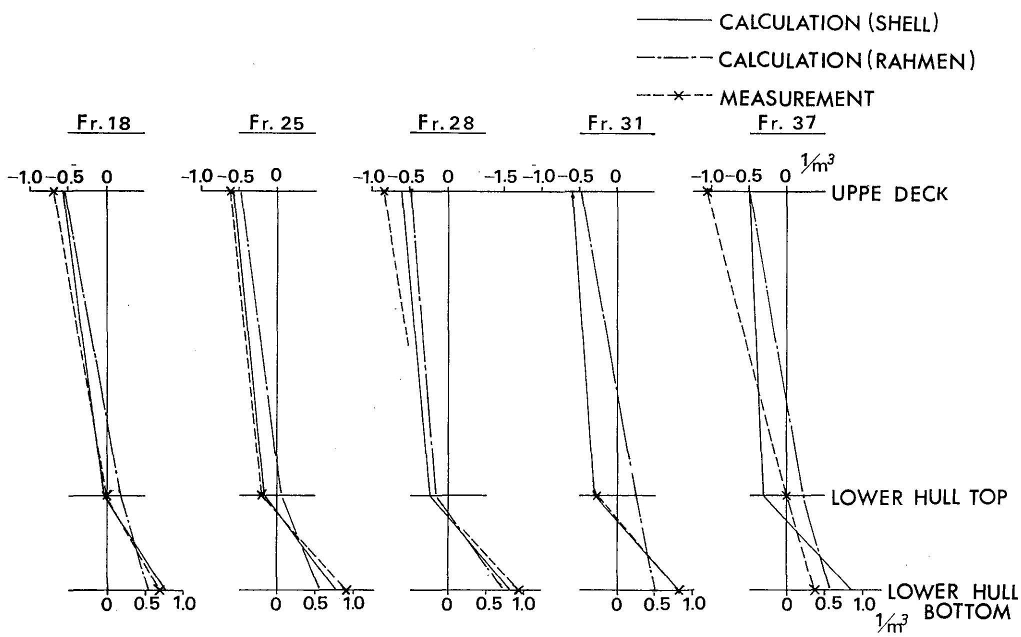

Fig. 18 Comparison between experiment and calculation
(Longitudinal bending stress/Longitudinal bending moment ×10)

considered to be a T-shape sectional member having equivalent sectional area and rigidity to that of actual structure. The segment of the structure was applied in the same manner as that of the time of launching.

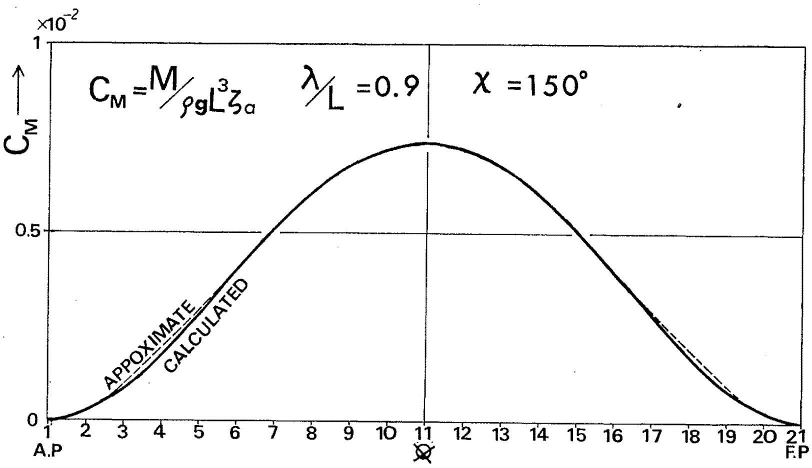

Fig. 19 Approximation of Longitudinal Bending Moment

5. Field Experiments of Loading Station

This Chapter presents comprehensive experiment of L. S. when being towed to Goa in India after completion.

The measurements were conducted during the period of December 28 to 30, 1971 from the offshore of Shikoku Island to the Kyushu Island. Measurement of waves was also conducted simultaneously.

5.1 Outline of the comprehensive experiment in the ocean

Fig. 20, and Fig. 21 and Table 2 indicate the general scheme of measuring system. After the observation boat reached to the area of experiment approximately two hours ahead of the L. S., wave measurement was conducted by the clover-leaf buoy about 30 minutes. When L. S. was towed to that area, the measuring instruments on L. S. was started remotely from the observation boat. At the same time the observation boat sailed in parallel to L. S., and the angle of encounter with waves and towing speed of L. S. were measured. The measurements of motion and stress of L. S. were continued for about 20 minutes, the measured data were recorded on magnetic tapes, which stopped automatically at designated time.

Thus, in some cases there were differences between measured data of L. S. and wave data, 30 to 90 minutes in time or maximum 6 km in distance as shown in Table 2. However, these differences did not affect so

Table 2 Measurement Date Table

MEASU EMRENT NO.	DATE	SEA DEPTH (m)	CLI-MATE	ATM. TEMP. (°C)	SEA WA-TER TEMP (°C)	WIND VELO CITY (m/sec)	WIND DIREC-TION	χ_p(°) MEAS-URED	χ_{pc}(°) APPLIED FOR SPECT-RAL CALCUL	TO-WING SPEED (knot)	L. S. MEASURE-MENT TIME	WAVE MEASURE-MENT TIME
1	'71-12-25											11:13-11:23
2	12-25											13:20-13:32
3	12-27											
4	12-28										10:41-10:46	
5	12-28	48	CLOUDY (10)	8.0	13.7	8.0	N	30～40		2	15:01-15:24	14:12-14:35
6	12-28											14:40-15:05
7	12-28							100～120		2	15:55-16:03	
8	12-28							100～120			16:??-17:15	
9	12-29	1500	FINE (1)	12.2	21.3	9.0	NNE	abt. 150	165	4～5	9:23- 9:49	9:00- 9:26
10	12-29							abt. 150		4.5	10:18-10:35	
11	12-29	2400	FINE (5)	14.2	21.2	7.0	NE	135～165	155	4～5	14:49-15:13	14:05-14:50
12	12-29							135～165			15:43-16:08	
13	12-30	3500	CLOUDY (10)	19.4	22.1	1.0	ENE	135～150	145	5.4	9:40-10:45	9:08-10:38
14	12-30										10:21-11:45	
15	12-30	4300	RAIN	18.2	21.6	9.0	NNW					13:40-14:05
16	12-30							135～150	140	4～5	15:21-15:40	

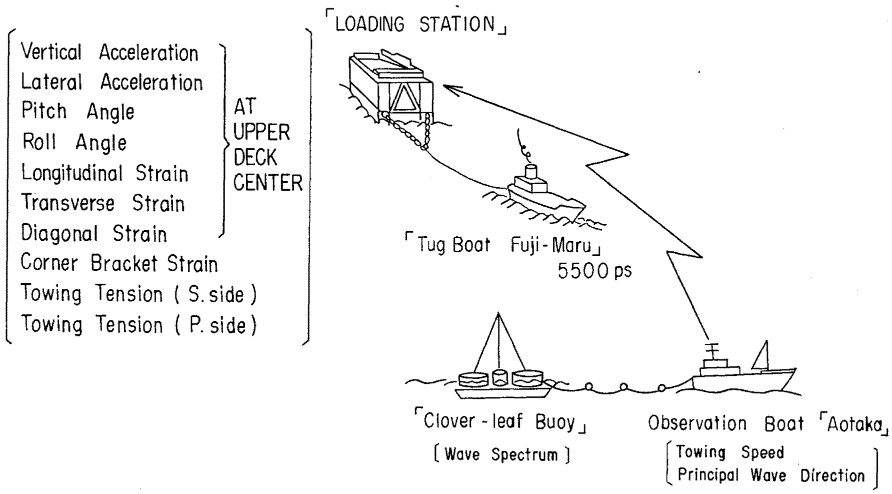

Fig. 20 Illustration of Comprehensive Experiment in the Ocean

much in the analysis because no rapid change of the weather was found during each observation.

5.2 The measurement and analysis of waves

The measurements of ocean waves were conducted by using the clover-leafbuoy newly developed by Research Institute for Applied Mechanics, Kyushu University. The buoy (See Fig. 22) is essentially the same type to that of the National Institute of Oceanography, which can measure the vertical acceleration, slope and carvature of the wave surface. The measured data are used for estimating, with high directional resolution, the directional spectrum:

$$E\ (f,\ \delta)=\phi\ (f)\cdot G\ (f,\ \delta),$$

where, ϕ (f) denotes one-dimensional spectrum defined by:

$$\varphi\ (f)=\int_{-\pi}^{\pi} E(f,\ \delta)\ \mathrm{d}\delta$$

and G (f, δ) denotes directional distribution function which indicates directional energy distribution of waves.

The collected wave data were digitized by using A-to-D converter (DATAC-500), and further processed on the FACOM 270-20 electronic computer system. The conditions for the data processing were as follows:

Data sampling interval: Approx. 0.34 sec.

Number of data of one group: 2,048

Length of data of one group: 11 min. 39 sec.

Spectral analsyis method: FFT
Used filter: Effective band width=0.043 Hz
Freedom of spectrum: Approx. 60

The one-dimensional wave spectrum of the measurement No. 16. are shown in Fig. 23.

As the result of analyzing all wave data measured this time, the following two facts were made obvious. First, for one-dimensional spectrum, spectrum having extrémely high concentration which is seen in wind wave

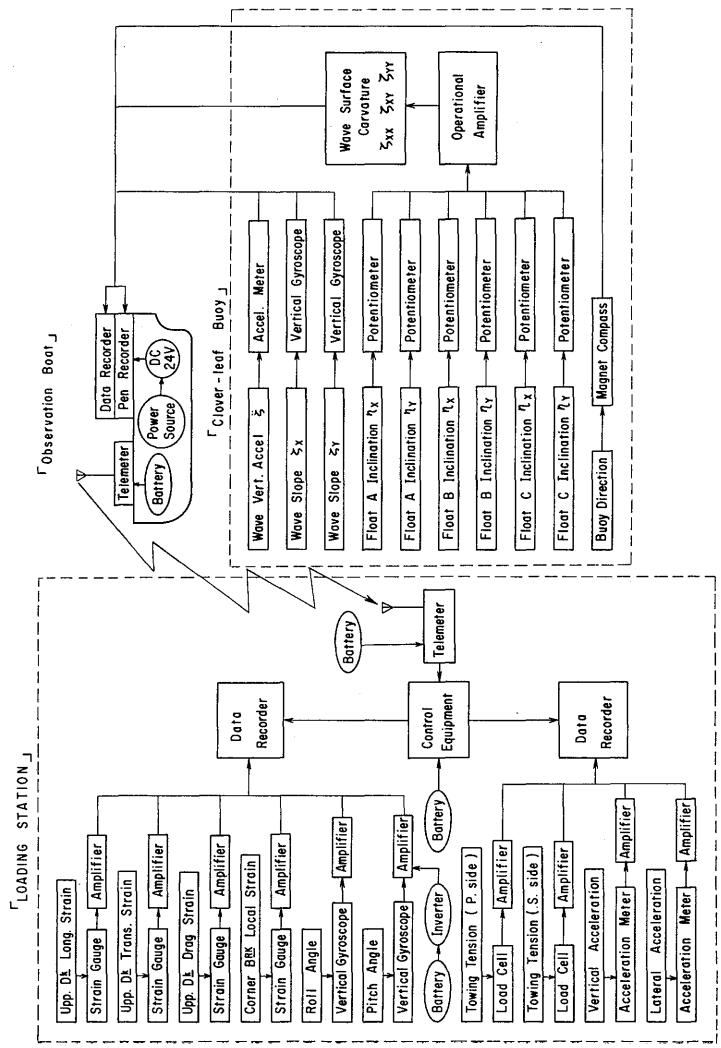

Fig. 21 Arrangement of Measuring Equipments

tank, spectrum having middle class of concentration which is frequently seen in waves generated in a bay, spectrum having comparatively small concentration which is represented by Pierson-Moskowitz's spectrum, and various other spectra exist in the ocean in accordance with the wave generating conditions.[7] Secondly, for the directional distribution function G (f, δ), the shape differs slightly depending upon frequency component of the waves. Directional distribution function of frequency component near the peak of the one-dimensional spectrum shows an extremely high concentration, and the concentration lowers rapidly in both lower and higher frequency sides of the spectrum. In other words, for the principal component waves which include much of wave energy, mean value of the wave directions is coincided with direction of the wind, and angular spreading is small. Mean value

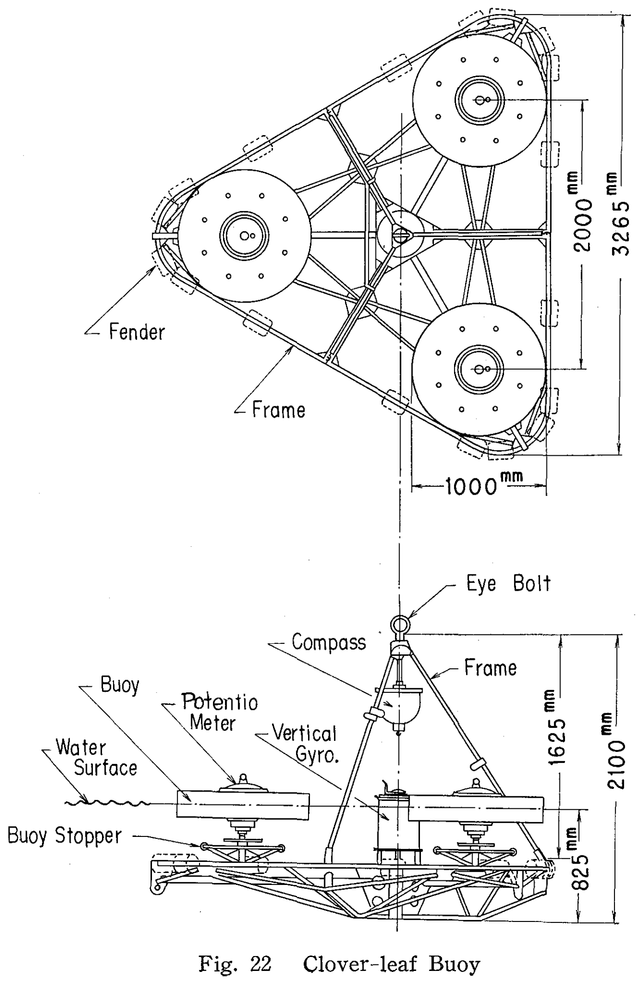

Fig. 22 Clover-leaf Buoy

of wave directions of the lower and higher frequency components having smaller energies is also coincided with the direction of wind; however, angular spreading is large.[8] Accordingly, estimating motion and longitudinal bending moment against the waves in the following section, the actually meas-

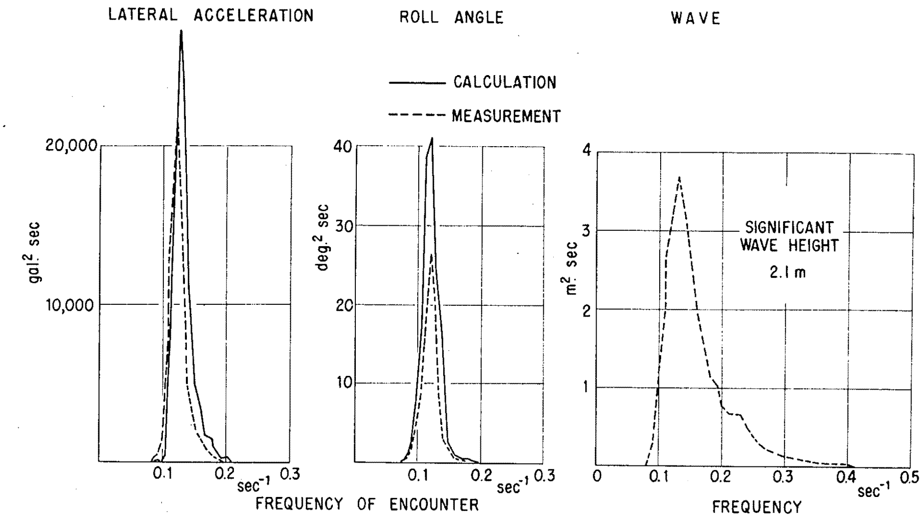

Fig. 23 One-Dimensional Wave Spectrum, and Comparison Between Calculated and Measured Spectra

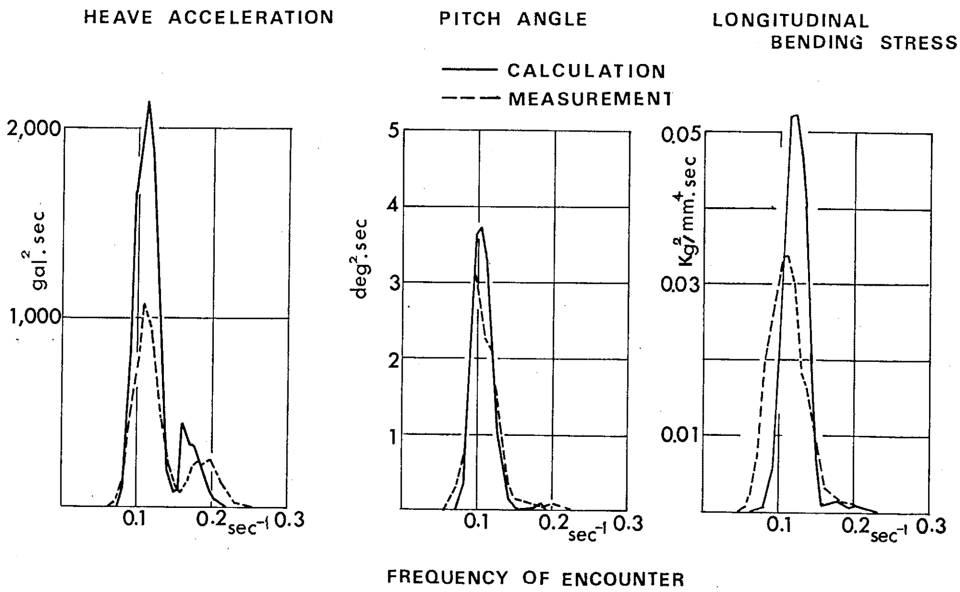

Fig. 24 Comparison between calcaulted and measured spectra

Table 3 Comparison between calculated and measured spectra (NO. 9, $\chi_{pc}=165°$, V=4KT)

ITEM	MODE	VERTICAL ACCELE-RATION	PITCH ANGLE	LATERAL ACCELE-RATION	ROLL ANGLE	LONGI-TUDINAL BENDING STRESS	WAVE
FREQUENCY IN WHICH POWER SPECTRUM DENCITY IS EXTREMUM (SEC^{-1})	CALCULATION	0.120	0.120	0.127	0.128	0.128	
	MEASUREMENT	0.112	0.120	0.120	0.120	0.116	0.16
EXTREMUM OF POWER SPECTRUM DENCITY	CALC.	482 $gal^2 \cdot sec$	1.46 $deg^2 \cdot sec$	12400 $gal^2 \cdot sec$	35.3 $deg^2 \cdot sec$	0.070 $kg^2/mm^4 \cdot sec$	
	MEAS.	108 $gal^2 \cdot sec$	0.434 $deg^2 \cdot sec$	2250 $gal^2 \cdot sec$	3.47 $deg^2 \cdot sec$	0.012 $kg^2/mm^4 \cdot sec$	4.37 $m^2 \cdot sec$
DOUBLE AMPLITUDE SIGNIFICANT VALUE	CALC. (A)	17.3gal	0.977deg	66.4gal	3.57deg	0.192 kg/mm^2	
	MEAS. (B)	12.1gal	0.520deg	32.2gal	1.36deg	0.100 kg/mm^2	2.06m
	A/B	1.43	1.89	2.06	2.63	1.92	

Table 4 Comparison between calculated and measured spectra (NO. 11, $\chi_{pc}=155°$, V=4KT)

ITEM	MODE	VERTICAL ACCELE-RATION	PITCH ANGLE	LATERAL ACCELE-RATION	ROLL ANGLE	LONGI-TUDINAL BENDING STRESS	WAVE
FREQUENCY IN WHICH POWER SPECTRUM DENCITY IS EXTREMUM (SEC^{-1})	CALCULATION	0.111	0.098	0.122	0.122	0.111	
	MEASUREMENT	0.104	0.105	0.120	0.127	0.115	0.14
EXTREMUM OF POWERSP ECTRUM DENCITY	CALC.	438 $gal^2 \cdot sec$	1.35 $deg^2 \cdot sec$	4080 $gal^2 \cdot sec$	10.9 $deg^2 \cdot sec$	0.032 $kg^2/mm^4 \cdot sec$	
	MEAS.	222 $gal^2 \cdot sec$	0.346 $deg^2 \cdot sec$	2920 $gal^2 \cdot sec$	4.07 $deg^2 \cdot sec$	0.006 $kg^2/mm^4 \cdot sec$	1.48 $m^2 \cdot sec$
DOUBLE AMPLITUDE SIGNIFICANT VALUE	CALC. (A)	17.2gal	0.772deg	42.4gal	2.20deg	0.121 kg/mm^2	
	MEAS. (B)	13.2gal	0.436deg	39.0gal	1.50deg	0.075 kg/mm^2	1.50m
	A/B	1.30	1.77	1.09	1.47	1.61	

Table 5 Comparison between calculated and measured spectra (NO. 13, $\chi_{pc}=145°$, V=5KT)

ITEM	MODE	VERTICAL ACCELERATION	PITCH ANGLE	LATERAL ACCELERATION	ROLL ANGLE	LONGITUDINAL BENDING STRESS	WAVE
FREQUENCY IN WHICH POWER SPECTRUM DENCITY IS EXTREMUM (SEC^{-1})	CALCULATION	0.119 0.162	0.097	0.126	0.119	0.132	
	MEASUREMENT	0.112 0.183	0.120	0.120	0.120	0.109	0.14
EXTREMUM OF POWER SPECTRUM DENCITY	CALC.	494 344gal^2·sec	1.04 deg^2·sec	9010 gal^2·sec	11.3 deg^2·sec	0.020 kg^2/mm^4·sec	
	MEAS.	232 390gal^2·sec	0.931 deg^2·sec	5550 gal^2·sec	9.33 deg^2·sec	0.013 kg^2/mm^4·sec	1.332 m^2·sec
DOUBLE AMPLITUDE SIGNIFICANT VALUE	CALC. (A)	20.4gal	0.76deg	61.8gal	2.42deg	0.107 kg/mm^2	
	MEAS. (B)	23.3gal	0.84deg	55.2gal	2.06deg	0.114 kg/mm^2	1.47m
	A/B	0.88	0.90	1.12	1.17	0.94	

Table 6 Comparison between calculated and measured spectra (NO. 16, $\chi_{pc}=140°$, V=4KT)

ITEM	MODE	VERTICAL ACCELERATION	PITCH ANGLE	LATERAL ACCELERATION	ROLL ANGLE	LONGITUDINAL BENDING STRESS	WAVE
FREQUENCY IN WHICH POWER SPECTRUM DENCITY IS EXTREMUM (SEC^{-1})	CALCULATION	0.113 0.160	0.105	0.127	0.120	0.120	
	MEASUREMENT	0.112 0.198	0.097	0.120	0.120	0.110	0.13
EXTREMUM OF POWER SPECTRUM DENCITY	CALC.	2120 440gal^2·sec	3.76 deg^2·sec	27500 gal^2·sec	41.3 deg^2·sec	0.052 kg^2/mm^4·sec	
	MEAS.	1060 260gal^2·sec	3.05 deg^2·sec	21600 gal^2·sec	26.7 deg^2·sec	0.034 kg^2/mm^4·sec	3.665 m^2·sec
DOUBLE AMPLITUDE SIGNIFICANT VALUE	CALC. (A)	38.1gal	1.44deg	106.8gal	4.46deg	0.180 kg/mm^2	
	MEAS. (B)	30.6gal	1.41deg	96.2gal	4.08deg	0.180 kg/mm^2	2.10m
	A/B	1.25	1.02	1.11	1.09	1.00	

ured values were used directly as the one-dimensional spectrum, and for the directional distribution function, in order to simplify the calculation, the following equation which is not related with the frequency was applied, because several problems still remain unsolved for the technological applications of the measured directional distribution functions:

$$G(\delta)=\frac{2}{\pi}\cos^2\delta \quad (|\delta|<\frac{\pi}{2}),$$

$$=0 \quad (|\delta|>\frac{\pi}{2}).$$

5.3 Spectral analysis of motion and stress and its results

Out of the total eleven measurements, nine measurements which were not affected by noises were analyzed. Table 3 through Table 6 and Fig. 23 and Fig. 24 indicate results of the analysis of the typical four cases.

The method of analysis was as follows:

(1) Calculation of power spectra

The measured data in analogue form were digitized at 200 Hz or 250 Hz with A-to-D converter (DATAC-1500), then power spectra were calculated using standard program based on a fast Fourier transform procedure. The conditions relating to the spectral analysis were almost the same to those for wave data.

(2) Conversions of power spectra

Within a frame work of linear theory, the ship-response spectrum can be given by[9]

$$S(f)=\int_{-\pi/2}^{\pi/2} E(f,\ \chi-\chi_{Pc})\ [A(f,\ \chi)]^2\, d\chi$$

where

$E(f,\ \chi-\chi_{Pc})$: Directional wave spectrum

$A(f,\ \chi)$: Frequency response function of ship hull

$S(f)$: Power spectral density of ship hull response

To compare this power spectral density S (f) estimated from the wave spectrum with the ones computed directly from measured data, it must be converted to the spectrum $S'(f_e)$ as a function of the frequency of encounter f_e. Because waves were measured at fixed point and the motion and stress of L. S. were measured in towing condition in the sea. That is, the following conversion of the spectrum is needed:

$$S'(f_e)=S(f)/(1+\frac{4\pi}{g}Vf\cos\chi)$$

In case of oblique following waves ($\chi>90°$), however, there occurs a difficult problem that at some frequencies power spectral density becomes infinite.[10] To cope with this the following approximation was made for converting the ship response spectra:

$$S'(f_e) = S(f)/(1+\frac{4\pi}{g}Vf\cos\chi_{pc})$$

With this assumption the difficulty in the calculation was eliminated for the present cases. For the case of No. 16 $\chi_{pc}=140°$ and V=4 knots, for example, converted spectrum becomes infinity at the frequency

$$f=0.495\ Hz, \qquad f_e=0.248\ Hz.$$

However, this was not so serious, because most of the power density of the ship hull response obtained for this case was in range of 0.23 Hz or below.

(3) Calculation of significant amplitude of the ship response

Let variance be $\sigma^2=\int_0^\infty S'(f_e)\,df_e$, the significant double amplitude is expressed by 4σ.

(4) Longitudinal bending stress

Time history of longitudinal bending stress $\sigma_x(t)$ was obtained from original data of longitudinal strain ε_x and transverse strain ε_y by the following equation:

$$\sigma_x=\frac{E}{1-\nu^2}(\varepsilon_x+\nu\varepsilon_y)$$

, where E is Young's modulous and ν is Poissonś ratio (0.3).
By using the value of σ_x thus obtained their spectra were calculated in the same procedure as in the other quantities.

6. Conclusion

The following important conclusions can be drawn from present investigation:

(1) Motion in irregular waves

Motions of floating marine structure with catamaran hulls in irregular waves can be estimated, with sufficient accuracy for engineering purpose, by the computations of response spectra utilizing the linear superposition principle, using the measured wave spectra and the response functions which are obtained by the strip method usually used for ship motions in oblique waves and are corrected by the results of model tank test.

(2) Strength in irregular waves

Longitudinal stress of the structure can be estimated with sufficient accuracy, by the finite element method of large size elements using the response function of longitudinal bending moment in waves which is also calculated by the strip method and partially corrected by the results of model tank test.

Acknowledgements

The authors are indebted to Mr. Masahiko Irie, Director & Manager, Technical Division of Mitsui Shipbuilding & Engineering Co., Ltd. and Mr. Minoru Nishikido, Chief of the Technical Division for their kind support during the period of research.

Reference

1) Suhara, T., Tasai, F., Mitsuyasu, H., Mutoh, I., Tanaka, E., Nakashima, K., Sao, K., Inaoka, K.: "Prediction of Motion and Strength of Floating Marine Structure in Waves", *OTC* (May 1974).
2) Mutoh, I.: "Mobile Offshore Bulk Transshipment Terminal", *Oceanology International 72 Conference Papers* (19/24 March, 1972, Brighton England).
3) Kobayashi, M., Yuasa, H., Kishimoto, O., Abe, M., Kunitake, Y., Narita, H., Hirano, M., Sugimura, Y.: "A Computer Program for Theoretical Calculation of Sea-Keeping Quality of Ships (Part 1-Method of Theoretical Calculation)", *MITSUI TECHNICAL REVIEW No. 82* (April 1973).
4) Ohkusu, M., Takaki, M.: "On the Motion of Twin Hull Ship in Waves", *I. N. S. A. of Japan Vol. 129* (June 1971).
5) Haskind, M.D.: "The exciting Forces and Wetting of Ships in Wave", (in Russian), *Izvestia Akademii Nauk U. S. S. R.*, Otdelenie Tekhnjech eskikh Nauk, No. 7, (1957), (English Translation available as *David Taylor Model Basin Translation No. 307*, (March, 1962).
6) Bessho, M.: "On the Theory of Rolling Motion of Ships among Waves", *Vol. 3, No. 1, Report of Scientific Research of Defence Academy.*
7) Mitsuyasu, H., Tasai, F., Suhara, T., Mizuno, Sh., Ohkusu, M., Honda, T., Rikiishi, K., Takaki, M., Hiyama, K.: "Studies on Technics of Ocean Wave Measurement (1)" *Rep. Res. Inst. for Appl. Mech., Kyushu Univ., No. 39* (March 1973)
8) Mitsuyasu, H., Tasai, F., Suhara, T., Mizuno, Sh., Ohkusn, M., Honda, T., Rikiishi, K.: "Studies on Technics of Ocean Wave Measurement (2)", *Rep. Res. Inst. for Appl. Mech., Kyushu Univ., No. 40* (1974)
9) Yamanouchi, Y.: "Ship Response in the Ocean Waves", *Symposium on Seakeeping, S.N.A. of Japan* (July 1969).
10) Takaishi, Y., Yoshino, T., Takagi, M., Saito, K.: "On the Motions of a High-Speed Container Ship with a Single Screw in Oblique Waves", *J. S. N. A. of Japan Vol. 129* (June 1971).

(Receved May 28, 1974)

Appendix A

In Fig. 25, O'-XYZ is a right-handed rectangular cartesian coordinate system fixed in the space. X and Y axes are taken on the calm water surface and Z axis is directed vertically downwards. O_0-$x_0y_0z_0$ is a right-handed rectangular cartesian coordinate system advancing with a constant speed V to a constant direction χ, and O_0 is taken on the O'-XY plane.

O-xyz and G-$x_b y_b z_b$ are right-handed rectangular cartesian coordinate systems fixed on a ship wiih the origin O at the midship and the origin G at the center of grairty . respectively. Wave direction χ and χ_{pc} are defined and illustrated in Fig. 26.

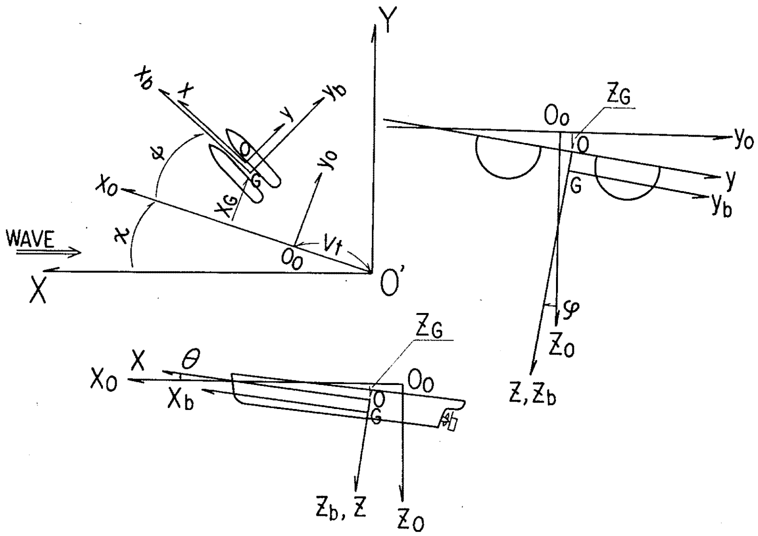

Fig. 25 Coordinate System

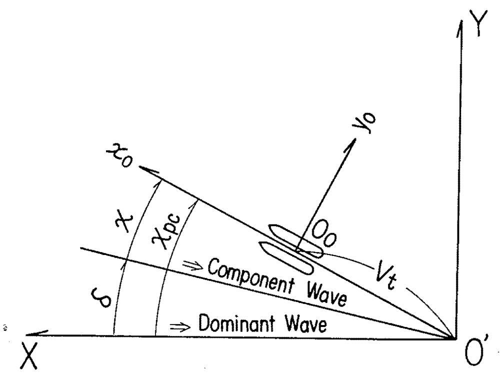

Fig. 26 Wave Direction

Appendix B

Hydrodynamic pressure is presented as follows:

$$P=\rho\left(\frac{\partial}{\partial t}-V\frac{\partial}{\partial x}\right)\phi+\rho g(z_G-x\theta)$$

By integrating the hydrodynamic pressure of radiation potential, diffraction potential and incident wave potential on the contour of the hull section, forces and moments acting on a hull per unit length can be obtained. Furthermore, by integrating stripwisely these forces or moments, coefficients of equation of motion and wave exciting forces or moments can be obtained.

(1) Longitudinal equation of motion

$$\begin{cases}(M+a_{zz})\ddot{z}_G+b_{zz}\dot{z}_G+c_{zz}z_G+a_{z\theta}\ddot{\theta}+b_{z\theta}\dot{\theta}+c_{z\theta}\theta=F_z\\(J_\theta+a_{\theta\theta})\ddot{\theta}+b_{\theta\theta}\dot{\theta}+c_{\theta\theta}\theta+a_{\theta z}\ddot{z}_G+b_{\theta z}\dot{z}_G+c_{\theta z}z_G=M_\theta\end{cases}$$

$$a_{zz}=\int M_H dx$$

$$b_{zz}=\int N_H dx-V[M_H]$$

$$c_{zz}=4\rho g\int b dx-V[N_H]$$

$$a_{z\theta}=-\frac{V}{\omega_e^2}\int N_H dx-\int xM_H dx$$

$$b_{z\theta}=-\int xN_H dx+V\int M_H dx+V[xM_H]+\frac{V^2}{\omega_e^2}[N_H]$$

$$c_{z\theta}=-4\rho g\int bx dx+V[xN_H]-V^2[M_H]$$

$$a_{\theta\theta}=\int x^2M_H dx$$

$$b_{\theta\theta}=\int x^2N_H dx+\frac{V^2}{\omega_e^2}\int N_H dx-V[x^2M_H]-\frac{V^2}{\omega_e^2}[xN_H]$$

$$c_{\theta\theta}=4\rho g\int bx^2 dx-V^2\int M_H dx-V[x^2N_H]+V^2[xM_H]$$

$$a_{\theta z}=-\int xM_H dx$$

$$b_{\theta z}=-\int xN_H dx-V\int M_H dx+V[xM_H]$$

$$c_{\theta z}=-4\rho g\int bx dx-V\int N_H dx+V[xN_H]$$

$$F_z=\zeta_w\omega\left\{i\int(N_H+i\omega_eM_H)e^{-KT_m}e^{ikx\cos\chi}dx-\frac{V}{\omega_e}\left[(N_H+i\omega_eM_H)e^{-KT_m}e^{ikx\cos\chi}\right]\right\}$$

$$+2\rho g\zeta_\omega\int e^{ikx\cos\chi}\int_{P-b}^{P+b}e^{-Kz}\cos(Ky\sin\chi)dydx$$

$$M_\theta=\zeta_w\omega\Big\{-\int\Big(ix+\frac{V}{\omega_e}(N_H+i\omega_e M_H)e^{-KT_m}e^{iKx\cos\chi}dx$$

$$+\frac{V}{\omega_e}[(N_H+i\omega_e M_H)e^{-KT_m}e^{iKx\cos\chi}x]\Big\}$$

$$-2\rho g\zeta_w\int e^{iKx\cos\chi}x\int_{P-b}^{P+b}e^{-Kz}cos(Ky\sin\chi)dydx$$

(2) Lateral equation of motion

$$\begin{cases}(M+a_{yy})\ddot{y}_G+b_{yy}\dot{y}_G+c_{yy}y_G+a_{y\phi}\ddot{\psi}+b_{y\phi}\dot{\psi}+c_{y\phi}\psi+a_{y\varphi}\ddot{\varphi}+b_{y\varphi}\dot{\varphi}+c_{y\varphi}\varphi=F_{ye}\\(J_\phi+a_{\phi\phi})\ddot{\psi}+b_{\phi\phi}\dot{\psi}+c_{\phi\phi}\psi+a_{\phi y}\ddot{y}_G+b_{\phi y}\dot{y}_G+c_{\phi y}y_G+a_{\phi\varphi}\ddot{\varphi}+b_{\phi\varphi}\dot{\varphi}+c_{\phi\varphi}\varphi=M_{\varphi e}\\(J_\varphi+a_{\varphi\varphi})\ddot{\varphi}+b_{\varphi\varphi}\dot{\varphi}+c_{\varphi\varphi}\varphi+a_{\varphi y}\ddot{y}_G+b_{\varphi y}\dot{y}_G+c_{\varphi y}y_G+a_{\varphi\phi}\ddot{\psi}+b_{\varphi\phi}\dot{\psi}+c_{\varphi\phi}\psi=M_{\varphi e}\end{cases}$$

$$a_{yy}=\int M_s dx$$

$$b_{yy}=\int N_s dx-V[M_s]$$

$$c_{yy}=-V[N_s]$$

$$a_{y\phi}=\int M_s x dx+\frac{V}{\omega_e^2}\int N_s dx$$

$$b_{y\phi}=\int N_s x dx-V\int M_s dx\frac{V^2}{\omega_e^2}[N_s]-V[xM_s]$$

$$c_{y\phi}=V^2[M_s]-V[xN_s]$$

$$a_{y\varphi}=\int M_{SR'}dx$$

$$b_{y\varphi}=\int N_{SR'}dx-V[M_{SR'}]$$

$$c_{y\varphi}=-V[N_{SR'}]$$

$$a_{\phi\phi}=\int M_S x^2 dx+\frac{V}{\omega_e^2}\int N_S x dx$$

$$b_{\phi\phi}=\int N_S x^2 dx+\frac{V^2}{\omega_e^2}\int N_S dx-\frac{V^2}{\omega_e^2}[yN_S]-V[x^2M_S]$$

$$c_{\phi\phi}=V\int N_S x dx-V^2\int M_S dx-V[x^2N_S]+V^2[xM_S]$$

$$a_{\phi\varphi}=\int M_{SR'}x dx$$

$$b_{\phi\varphi}=\int N_{SR'}x dx+V\int M_{SR'}dx-V[xM_{SR'}]$$

$$c_{\phi\phi}=V\int N_{SR'}dx-V[xN_{SR'}]$$

$$a_{\phi y}=\int M_S x dx$$

$$b_{\phi y}=\int N_S x dx+V\int M_S dx-V[xM_S]$$

$$c_{\phi y}=V\int N_S dx-V[xN_S]$$

$$a_{\varphi\varphi}=\int M_{R'}dx \qquad M_{R'}=M_R+2\cdot\overline{OG}\cdot M_{SR}+\overline{OG}^2\cdot M_S$$

$$b_{\varphi\varphi}=\int N_{R'}dx-V[M_{R'}] \qquad N_{R'}=N_R+2\cdot\overline{OG}\cdot N_{SR}+\overline{OG}\cdot N_S$$

$$c_{\varphi\varphi}=W\cdot GM-V[N_{R'}]$$

$$a_{\varphi y}=\int M_{SR'}dx$$

$$b_{\varphi y}=\int N_{SR'}dx-V[M_{SR'}]$$

$$c_{\varphi y}=-V[N_{SR'}]$$

$$a_{\varphi\phi}=\frac{V}{\omega_e^2}\int N_{SR'}dx+\int M_{SR'}xdx$$

$$b_{\varphi\phi}=\int N_{SR'}dx-V\int M_{SR'}dx-\frac{V^2}{\omega_e^2}[N_{SR'}]-V[xM_{SR'}]$$

$$c_{\varphi\phi}=V^2[M_{SR'}]-V[xN_{SR'}]$$

$$F_y=-\zeta_w\omega\sin\chi\Big\{\int(N_{SR}+i\omega_e M_{SR})e^{-KT_m}e^{iKx\cos\chi}dx$$

$$+i\frac{V}{\omega_e}[(N_{SR}+i\omega_e M_{SR})e^{-KT_m}e^{iKx\cos\chi}]\Big\}$$

$$+i2\rho g\zeta_w\int e^{iKx\cos\chi}\int_{GR}e^{-Kz}\sin(Ky\sin\chi)dzdx$$

$$M_\phi=-\zeta_w\omega\sin\chi\Big\{\int(N_S+i\omega_e M_S)\Big(x-i\frac{V}{\omega_e}\Big)e^{-KT_m}e^{iKx\cos\chi}dx$$

$$+i\frac{V}{\omega_e}[N_S+i\omega_e M_S)e^{-KT_m}e^{iKx\cos\chi}]\Big\}$$

$$+i2\rho g\zeta_w\int e^{tKx\cos\chi}x\int_{GR}e^{-Kz}\sin(Ky\sin\chi)dzdx$$

$$M_\varphi=-\zeta_w\omega\sin\chi\Big\{\int(N_{SR'}+i\omega_e M_{SR'})e^{-KT_m}e^{iKx\cos\chi}dx$$

$$+i\frac{V}{\omega_e}[N_{SR'}+i\omega_e M_{SR'})e^{-KT_m}e^{iKx\cos\chi}]\Big\}$$

$$-i2\rho g\zeta_w\int e^{iKx\cos\chi}\int_{GR}e^{-Kz}\sin(Ky\sin\chi)\{(z-\overline{OG})dz+ydy\}dx$$

where, each equation or coefficient to be for the condition of $\otimes G=0$, and in the case of $\otimes G\neq 0$, every integrated function χ to be converted as $\chi-\otimes G$,

(3) Longitudinal wave shearing force

Longitudinal wave shearing force acting on a unit length at arbitrary section x is presented as follows, considering all vertical hydrodynamic forces, that is, inertia force, radiation force, Froude-Kriloff's force and diffraction force:

$$F_z(x)=\ddot{\theta}\left\{\frac{V}{\omega_e^2}\int_{la}^{xl} N_H\,dx+\int_{la}^{x} xM_H\,dx+\int_{la}^{x}\frac{w}{g}dx\right\}$$

$$+\dot{\theta}\left\{\int_{la}^{x} xN_H\,dx-V\int M_H\,dx-V\Big[xM_H\Big]_{la}^{x}+\frac{V^2}{\omega_e^2}\Big[N_H\Big]_{la}^{x}\right\}$$

$$+\theta\left\{4\rho g\int_{la}^{x} b\,dx-V\Big[xN_H\Big]_{la}^{x}+V^2\Big[N_H\Big]_{la}^{x}\right\}$$

$$-\ddot{z}_G\left\{\int_{la}^{x} M_H dx+\int_{la}^{x}\frac{w}{g}dx\right\}-\dot{z}_G\left\{\int_{la}^{x} N_H dx-V\Big[M_H\Big]_{la}^{x}\right\}$$

$$-z_G\left\{4\rho g\int_{la}^{x} bx\,dx-V\Big[N_H\Big]_{la}^{x}\right\}$$

$$\zeta_w\omega\left\{i\int_{la}^{x}(N_H+i\omega_e M_H)e^{-KT_m}e^{iKx\cos\chi}dx\right.$$

$$-\frac{V}{\omega_e}\Big[(N_H+i\omega_e M_H)\,e^{-KT_m}\,e^{iKx\cos\chi}\Big]_{la}^{x}$$

$$+2\rho g\zeta_w\int_{la}^{x} e^{iKx\cos\chi}\int_{P-b}^{P+b} e^{-Kz}\cos(Ky\sin\chi)\,dy\,dx$$

(4) Longitudinal wave bending moment

Longitudinal wave bending moment acting on a unit length at χ' section is presented as follows:

$$M(x')=-\ddot{\theta}\left\{\int_{la}^{x'} M_H x^2\,dx+\int_{la}^{x'}\frac{w}{g}x^2dx\right\}$$

$$-\dot{\theta}\left\{\int_{la}^{x'} N_H x^2\,dx+\frac{V^2}{\omega_e^2}\int_{la}^{x'} N_H dx-V\Big[x^2M_H\Big]_{la}^{x'}-\frac{V^2}{\omega_e^2}\Big[xN_H\Big]_{la}^{x'}\right\}$$

$$-\theta\left\{4\rho g\int_{la}^{x'} bx^2\,dx-V^2\int_{la}^{x'} M_H dx-V\Big[x^2N_H\Big]_{la}^{x'}+V^2\Big[xM_H\Big]_{la}^{x'}\right\}$$

$$+\ddot{z}_G\left\{\int_{la}^{x'} xM_H dx+\int_{la}^{x'}\frac{w}{g}x\,dx\right\}+\dot{z}_G\left\{\int_{la}^{x'} xN_H dx+V\int_{la}^{x'} M_H dx-V\Big[xM_H\Big]_{la}^{x'}\right\}$$

$$+z_G\left\{4\rho g\int_{la}^{x'} bx\,dx+V\int_{la}^{x'} N_H dx-V\Big[xN_H\Big]_{la}^{x'}\right\}$$

$$+\zeta_w\omega\left\{-\int_{la}^{x'}\left(ix+\frac{V}{\omega_e}\right)(N_H+i\omega_e M_H)e^{-KT_m}e^{iKx\cos\chi}dx\right.$$

$$\left.+\frac{\omega}{\omega_e}V\Big[(N_H+i\omega_e M_H)\,x e^{-KT_m}e^{iKx\cos\chi}\Big]_{la}^{x'}\right\}$$

$$-2\rho g\zeta_w\int_{la}^{x'} e^{iKx\cos_\chi}x\int_{P-b}^{P+b} e^{-Kz}\cos(Ky\sin\chi)\,dy\,dx+x'F_z(x')$$